1672

JUNE 1980

PPPL-1672
UC-20g

TEMPORAL EVOLUTION OF LOWER HYBRID WAVES IN THE PRESENCE OF PONDEROMOTIVE DENSITY FLUCTUATIONS

BY

C. F. F. KARNEY

PLASMA PHYSICS LABORATORY

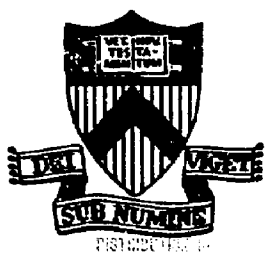

PRINCETON UNIVERSITY
PRINCETON, NEW JERSEY

This work was supported by the U.S. Department of Energy Contract No. DE-AC02-76-CHO 3073.

Jun : 1980

Temporal evolution of lower hybrid waves in the presence of ponderomotive density fluctuations

Charles F. F. Karney

Plasma Physics Laboratory, Princeton University,
Princeton, New Jersey 08544

The propagation of lower hybrid waves in the presence of ponderomotive density fluctuations is considered. The problem is treated in two dimensions and, in order to be able to correctly impose the boundary conditions, the waves are allowed to evolve in time. The fields are described by $iv_\tau - \int v_\xi \, d\zeta + v_{\zeta\zeta} + |v|^2 v = 0$ where v is proportional to the electric field, τ to time, and ζ and ξ measure distances across and along the lower hybrid ray. The behavior of the waves is investigated numerically. If the amplitude of the waves is large enough, the spectrum of the waves broadens and their parallel wavelength becomes shorter. The assumptions made in the formulation preclude the application of these results to the lower hybrid heating experiment on Alcator–*A*. Nevertheless, there are indications that the physics embodied in this problem are responsible for some of the results of that experiment.

I. INTRODUCTION

The injection of rf power near the lower hybrid frequency is an attractive method for the auxiliary heating of tokamak plasmas.[1] Because of the high powers required (several MW) and because lower hybrid waves principally propagate along well-defined resonance cones,[2-4] there has been considerable interest in nonlinear effects on the propagation of lower hybrid waves. This problem was first addressed by Morales and Lee[5] who studied the two-dimensional electrostatic propagation of one of the two lower hybrid rays in a homogeneous plasma. Although this is perhaps the simplest model that can be considered, a correct treatment of this problem has yet to be made. It is this deficiency that this paper attempts to remedy.

Briefly the difficulty of this problem arises as follows: If it is assumed that the rf fields in the plasma have reached a steady state, i.e., that the potential is given by $\phi(x,z)\exp(-i\omega_0 t)$ (x and z are coordinates perpendicular and parallel to the ambient magnetic field B_0), then the electric field obeys the complex modified Korteweg-deVries equation.[5-7] This equation is mathematically well-posed when solved as an initial value problem in one of the coordinates z, that is when $\phi(z = 0, z)$ is given. Unfortunately, this does not correspond to physically realizable boundary conditions since waves can propagate in both the $+z$ and $-z$ directions in a single ray.[7, 8] When the correct boundary conditions are imposed, there is numerical evidence that solutions of the complex modified Korteweg-deVries equation need not exist and that this equation is therefore ill-posed.[7] This is confirmed by our finding solutions inconsistent with the assumption of a steady state (see Sec. IV). The problem arises because the direction of power flow which determines how to impose the boundary conditions is defined only with reference to a problem in which a temporal evolution of the wave packet is allowed. In assuming a steady state for the electric field amplitude, the equation no longer has built into it the crucial ingredient which determines how the boundary conditions are imposed. This defect is corrected by including a slow time dependence of the potential [so that the potential is given by $\phi(x,z,t)\exp(-i\omega_0 t)$]. This then leads to a nonlinear partial differential equation in two spatial dimensions and time, which we will study numerically in this paper.

In formulating this problem, we shall ignore many effects which should possibly be included to obtain a complete understanding of the propagation of lower hybrid waves. This will enable us to study the effect of the nonlinearity in as simple a system as possible. Even so, the numerical solution of a partial differential equation in two dimensions and time is time consuming and, as we shall see, the behavior of the fields as described by this equation can be quite complicated. In the absence of any analytical methods for solving this equation, we must therefore be content with the solution for only a few cases. This will enable us to confirm the threshold for strong nonlinear effects given in Ref. 7 and to give a more complete description of the nature of these nonlinear effects. Because of the approximations made in formulating the problem, we shall not be able to apply these results to the propagation of lower hybrid waves near the edge of a tokamak plasma where nonlinear effects are most strong. However, there are indications that the physical processes that are considered in this paper do play a role in the propagation in that region.

The plan of this paper is as follows: In Sec. II we derive the partial differential equation governing the temporal evolution of ϕ. The basic properties of this equation will be discussed in Sec. III. In particular, we will show how the right boundary conditions automatically drop out from the equation.

Since the equation is analytically intractable, we resort to a numerical integration, the results of which are given in Sec. IV. The threshold condition for a strong nonlinear interaction is derived in Sec. V. The results are summarized and the consequences to lower hybrid heating of tokamaks are presented in Sec. VI.

II. FORMULATION OF THE PROBLEM

In this section, we derive the partial differential equation governing the evolution of the electric field for one of the lower hybrid rays in two spatial dimensions and time. We assume that the fields are electrostatic, that the plasma is homogeneous, and that it is immersed in a uniform magnetic field. The derivation closely follows that of the complex modified Korteweg–deVries equation by Morales and Lee;[5] the additional ingredient we consider is the slow time dependence of ϕ.

The potential of the lower hybrid wave is taken to have the form

$$\mathrm{Re}[\phi(x,z,t)\exp(-i\omega_h t)]$$

where the t dependence of ϕ is taken to be much slower than ω_h. Since we are only doing the two-dimensional problem, we have $\partial/\partial y \equiv 0$. In the electrostatic limit, ϕ obeys Poisson's law

$$\nabla \cdot \mathbf{K}(\nabla, \partial/\partial t, |\nabla\phi|^2) \cdot \nabla\phi = 0. \tag{1}$$

Here we regard the dielectric tensor $\mathbf{K}$ as an operator through its arguments ∇ and $\partial/\partial t$. The dependence on $|\nabla\phi|^2$ accounts for the nonlinearity. If the temporal evolution of ϕ is sufficiently slow (compared with ion acoustic time scales), then nonlinearities due to ponderomotive density changes can be written in this way. Parametric instabilities are excluded from our consideration.

If the dependence of ϕ on x, z, and t is weak and if the ϕ itself is small so that the nonlinearity is weak, we may expand $\mathbf{K}$ to obtain

$$\mathbf{K}(\nabla, \partial/\partial t, |\nabla\phi|^2) = \mathbf{K} + \tfrac{1}{2}\epsilon \frac{\partial^2 \mathbf{K}}{\partial\nabla\partial\nabla} : \nabla\nabla + \epsilon \frac{\partial \mathbf{K}}{\partial(\partial/\partial t)} \frac{\partial}{\partial t} + \epsilon \frac{\partial \mathbf{K}}{\partial|\nabla\phi|^2} |\nabla\phi|^2 + O(\epsilon^2). \tag{2}$$

All the evaluations of $\mathbf{K}$ on the right hand side of Eq. (2) are at the point $\nabla = \partial/\partial t = |\nabla\phi|^2 = 0$. The term involving $\partial\mathbf{K}/\partial\nabla$ is zero because of the symmetries of a stationary plasma. We have introduced a formal expansion parameter ϵ to aid in the ordering of terms. The fact that the last three terms in Eq. (2) are taken to be of order ϵ results a maximal ordering. If, in fact, one of the terms is much smaller than the others, a subsidiary ordering can be introduced to eliminate that term.

Since it is more usual to write $\mathbf{K}$ as a normal function, rather than as an operator, we rewrite $\mathbf{K}$ as $\mathbf{K}(\mathbf{k}, \omega, n)$ where $\mathbf{k}$ is the Fourier-transform variable conjugate to space, ω is that conjugate to time, and n is the plasma density. [A space-time dependence of $\exp\{i\mathbf{k}\cdot\mathbf{r} - i\omega t\}$, where $\mathbf{r} = (x, z)$, is assumed.] Then the derivatives in Eq. (2) become

$$\frac{\partial^2 \mathbf{K}}{\partial\nabla\partial\nabla} = -\frac{\partial^2 \mathbf{K}}{\partial\mathbf{k}\partial\mathbf{k}}, \qquad \frac{\partial \mathbf{K}}{\partial(\partial/\partial t)} = i\frac{\partial \mathbf{K}}{\partial\omega}, \qquad \frac{\partial \mathbf{K}}{\partial|\nabla\phi|^2} = \frac{\partial n}{\partial|\nabla\phi|^2}\frac{\partial \mathbf{K}}{\partial n}.$$

In this case, all the evaluations on the right hand sides are performed at $\mathbf{k} = 0$, $\omega = \omega_0$, and $n = n_0$, where n_0 is the unperturbed density of the plasma (i.e., in the absence of any electric fields).

We now write down Eq. (1) to various orders in ϵ. To order ϵ^0, we find

$$\nabla \cdot \mathbf{K}(0, \omega_0, n_0) \cdot \nabla \phi = 0 \tag{3}$$

where

$$\mathbf{K}(0, \omega_0, n_0) = \begin{pmatrix} K_\perp & 0 \\ 0 & K_\parallel \end{pmatrix}.$$

Assuming that $K_\perp K_\parallel$ is negative, Eq. (3) is hyperbolic and its solution is

$$\phi = \phi_+(x - gz) + \phi_-(x + gz)$$

where $g = (-K_\perp/K_\parallel)^{1/2}$.

In general, both the right- and left-going rays will be present. However, if the source of the lower hybrid rays is localized, the two rays will be separated far from the source and in that region we may then treat each ray in isolation. Similarly, only a single ray will be present if the source is adjusted so that only that ray is excited. We may therefore assume that, to zeroth order, only the right-going ray is present, i.e., $\phi_- = 0$. To order ϵ^1, we write $\phi = \phi(\epsilon t', \epsilon x', z')$ where $t' = t$, $x' = x$, $z' = cz - sx$, and $s = (1 + g^2)^{-1/2}$, $c = gs$. We should think of x' and z' as measuring distances along and across the lower hybrid ray. Substituting this form of ϕ into Eq. (1), we obtain to order ϵ^1

$$iA\frac{\partial^2 E}{\partial x' \partial t'} - B\frac{\partial E}{\partial x'} + C\frac{\partial^3 E}{\partial z'^3} + D\frac{\partial}{\partial z'}(|E|^2 E) = 0 \tag{4}$$

where $E = \partial\phi/\partial z'$ is the electric field measured in the direction normal to the lower hybrid ray, A, B, C, and D are real coefficients given by

$$A = \hat{\mathbf{k}} \cdot \frac{\partial \mathbf{K}}{\partial \omega} \cdot \hat{\mathbf{k}}, \qquad B = 2sK_\perp,$$

$$C = -\frac{1}{2}\hat{\mathbf{k}}\hat{\mathbf{k}} : \frac{\partial^2 \mathbf{K}}{\partial \mathbf{k} \partial \mathbf{k}} : \hat{\mathbf{k}}\hat{\mathbf{k}}, \qquad D = -\frac{1}{n}\frac{\partial n}{\partial |\nabla \phi|^2},$$

and $\hat{\mathbf{k}}$ is the unit vector $(-s, c)$.

These expressions may be evaluated using the expression for $\mathbf{K}$ for a stationary Maxwellian plasma.[9] Usually the frequency of the incident rf power satisfies $\Omega_i^2 \ll \omega_0^2 \ll \Omega_e^2$ where Ω_j is the cyclotron frequency of species j ($j = i$ or e for ions or electrons). In that case, the components of the zeroth-order dielectric tensor may be written

$$K_\perp = 1 + \frac{\omega_{pe}^2}{\Omega_e^2} - \frac{\omega_{pi}^2}{\omega_0^2}, \qquad K_\parallel = 1 - \frac{\omega_{pe}^2}{\omega_0^2} - \frac{\omega_{pi}^2}{\omega_0^2},$$

where ω_{pj} is the plasma frequency for species j with density n_0. The coefficients in Eq. (4) become

$$A = \frac{2}{\omega_0}\left(1 + \frac{\omega_{pe}^2 + \omega_{pi}^2}{\Omega_e^2}\right),$$

$$C = 3\frac{\omega_{pi}^2 v_{ti}^2}{\omega_0^4} + \frac{3}{4}s^4\frac{\omega_{pe}^2 v_{te}^2}{\Omega_e^4} - s^2c^2\frac{\omega_{pe}^2 v_{te}^2}{\omega_0^2\Omega_e^2} + 3c^4\frac{\omega_{pe}^2 v_{te}^2}{\omega_0^4},$$

$$D = \frac{1}{4}\frac{\epsilon_0}{n_0(T_e + T_i)},$$

where $v_{tj}^2 = T_j/m_j$, T_j is the temperature of species j, and ϵ_0 is the dielectric constant of free space. In writing the expression for D, we have used the formula for the density depression due to the ponderomotive force.[5, 10, 11] Note that C is always positive. The fact that C and D have the same signs has an important effect on the propagation of the lower hybrid waves.

We now rescale the variables in Eq. (4):

$$\xi = x'/(B\sqrt{C}), \quad \tau = t'/A, \quad \varsigma = z'/\sqrt{C}, \quad v = \sqrt{D}E. \tag{5}$$

The equation for v is then

$$iv_\tau - \int_{-\infty}^{\varsigma} v_\xi\, d\varsigma + v_{\varsigma\varsigma} + |v|^2 v = 0 \tag{6a}$$

where subscripted Greek letters denote differentiation. When integrating Eq. (4) to give Eq. (6a), we assume that v and all its derivatives are zero at $\varsigma = -\infty$ (i.e., far from the ray). The accessibility condition[12] imposes an auxiliary condition on v namely

$$\int_{-\infty}^{\infty} v\, d\varsigma = 0; \tag{6b}$$

in other words, the electric potential is equal at $\varsigma = \pm\infty$. Equation (6) describes the evolution of the electric field of a single lower hybrid ray in two dimensions and time under the influence of thermal dispersion and nonlinear ponderomotive effects. Equation (6a) is the same as Eq. (50) of Ref. 7 if the replacements $v \to v^*$, $\sigma \to \tau$, $\tau \to \xi$, and $\xi \to -\varsigma$ are made to the latter equation.

In order to give some appreciation of the scaling of the variables in Eq. (5), we give more explicit forms for them in the limit $\omega_{pi}^2 \ll \omega_0^2 \ll \omega_{pe}^2 \ll \Omega_e^2$ and $T_i \ll T_e$ (these may be the conditions applicable as the lower hybrid wave propagates through the low density part of a tokamak plasma). Equation (5) then becomes

$$\xi = \frac{x}{2\sqrt{3}\lambda_{De}}, \quad \tau = \frac{\omega_0 t}{2}, \quad \varsigma = \frac{gz - x}{\sqrt{3}\lambda_{De}}, \quad v = \left(\frac{\epsilon_0}{4n_0T_e}\right)^{1/2}E, \tag{7}$$

where $\lambda_{De} = v_{te}/\omega_{pe}$ is the Debye length and $g = \omega_0/\omega_{pe}$.

III. BASIC PROPERTIES OF THE EQUATION

Equation (6) is invariant under the scaling transformation

$$\xi \to \lambda^{-3}\xi, \qquad \tau \to \lambda^{-2}\tau, \qquad \zeta \to \lambda^{-1}\zeta, \qquad v \to \lambda v. \tag{8}$$

This invariance allows us, for example, to normalize the scale length of the ray in the ζ direction to unity.

If we set $\partial/\partial\tau = 0$ in Eq. (6), we obtain, as expected, the complex modified Korteweg–deVries equation as the equation obeyed by steady-state fields. If $\partial/\partial\xi = 0$, we obtain the nonlinear Schroedinger equation, which is soluble by the inverse scattering method.[13] Unfortunately, not much use can be made of this fact because, as we shall see, the imposition of the correct boundary conditions involves solving Eq. (6) in a finite domain in ξ.

For each of the four conservation laws obtained for the complex modified Korteweg–deVries equation, there is a corresponding conservation law for Eq. (6). These are given in Table I. The second and third of these laws are statements of the conservation of momentum and energy respectively. We will return to these shortly.

In order to determine the correct boundary conditions for Eq. (6), we Fourier transform in ζ. Defining the Fourier transform of v by

$$V(\xi, \kappa, \tau) = \int_{-\infty}^{\infty} v(\xi, \zeta, \tau) \exp(-i\kappa\zeta)\, d\zeta$$

we obtain

$$V_\tau + cV_\xi + i\Omega V + iN(V) = 0, \tag{9a}$$

$$V(\kappa = 0) = 0, \tag{9b}$$

where $c = 1/\kappa$, $\Omega = \kappa^2$, and $N(V)$ is the Fourier transform of $-|v|^2 v$. This equation is hyperbolic in (τ, ξ) space. However, the direction of the characteristic velocity c depends on κ. This means that we must specify boundary conditions at each end of a strip in ξ. More precisely, the full initial and boundary conditions required for solving Eq. (9) in the domain

$$\xi_0 < \xi < \xi_1, \qquad -\infty < \zeta < \infty, \qquad \tau_0 < \tau < \infty$$

are

$$V(\xi_0 < \xi < \xi_1, \kappa, \tau_0), \quad V(\xi_0, \kappa > 0, \tau > \tau_0), \quad V(\xi_1, \kappa < 0, \tau > \tau_0). \tag{10}$$

Taking the second and fourth conservation laws in Table I, integrating them over ζ and ξ, and transforming them to κ space, we obtain the laws of conservation of momentum and energy as they apply to the domain of the problem

$$\frac{d}{d\tau}\int_{\xi_0}^{\xi_1}\int_{-\infty}^{\infty} \mathcal{M}\, d\kappa\, d\xi + \int_{-\infty}^{\infty} \mathcal{P}\, d\kappa \Big|_{\xi=\xi_0}^{\xi_1} = 0, \tag{11}$$

$$\frac{d}{d\tau}\int_{\xi_0}^{\xi_1}\int_{-\infty}^{\infty} \mathcal{E}\, d\kappa\, d\xi + \int_{-\infty}^{\infty} \mathcal{P}\, d\kappa \Big|_{\xi=\xi_0}^{\xi_1} = 0, \tag{12}$$

where $\mathcal{M} = \kappa|V|^2$ is the spectral momentum density, $\mathcal{F} = c\mathcal{M}$ is the spectral force density, $\mathcal{E} = |V|^2$ is the spectral energy density, and $\mathcal{P} = c\mathcal{E}$ is the spectral power density. The characteristic velocity c is the group velocity of the lower hybrid waves. The boundary conditions given in Eq. (10) stipulate that we should specify the waves entering the domain of the problem, but not those that leave this domain.

Given that we are treating a nonlinear problem, it may be a little surprising the boundary conditions are applied in the same way as for the corresponding linear problem. The reason for this is that, in deriving Eq. (6), we assumed that the nonlinear term was very small. The expressions for the energy density, power density, etc. are therefore correctly given by linear theory. Although the nonlinearity is small, it can have a finite effect because the ordering also assumes that the length over which the interaction takes place is large.

Notice that the nature of the equation has forced us to take boundary conditions which are in accord with physical notions of power flow. This has happened because we have the time variation in Eq. (6). If we consider the steady-state equation, the complex modified Korteweg–deVries equation, which is obtained by setting $\partial/\partial\tau = 0$ in Eq. (6)

$$v_\xi - v_{\varsigma\varsigma\varsigma} - (|v|^2 v)_\varsigma = 0, \tag{13}$$

then we would clearly like to impose the same boundary conditions as for Eq. (6) namely Eq. (10). But the concept of power flow cannot be defined from Eq. (13) and so there is no guarantee that the boundary conditions given in Eq. (10) are sensible. Indeed, the evidence of Ref. 7 suggests that Eq. (13) is ill-posed with these boundary conditions. This can be so because, even if Eq. (6) is given steady-state boundary conditions, i.e.,

$$V(\xi_0 < \xi < \xi_1, \kappa, \tau_0 \to -\infty), \quad \frac{\partial}{\partial\tau} V(\xi_0, \kappa > 0, \tau) = \frac{\partial}{\partial\tau} V(\xi_1, \kappa < 0, \tau) = 0,$$

it is not necessarily the case that the solution to Eq. (6) approaches a steady state.

As mentioned in Sec. II, the ordering we used in deriving Eq. (6) was a maximal ordering. We can eliminate some of the terms in Eq. (6) using a subsidiary ordering. E.g., the linear limit is obtained by letting $v \to \delta v$ and taking the limit $\delta \to 0$. Similarly, the non-dispersive limit is obtained by letting $\varsigma \to \varsigma/\delta$, $\xi \to \xi/\delta$ and again taking the limit $\delta \to 0$. It is instructive to examine this case in more detail because there are indications that if $\xi_1 - \xi_0$ is sufficiently large then the dispersive term must be included. Consider the steady-state equation (13) without the dispersive term $v_{\varsigma\varsigma\varsigma}$. Multiplying this equation by v^* and adding the complex conjugate (these are the same operations that lead to the second conservation law in Table I), we obtain

$$u_\xi + uu_\varsigma = 0 \tag{14}$$

where $u = 3|v|^2$. Since the boundary conditions involve $\arg v$, Eq. (14) should be supplemented by another equation. However, this is not so if we impose initial conditions $v(\xi = \xi_0, \varsigma)$. As is well known, the solution develops a shock at $\xi = \xi_0 + 1/\max|du(\xi = \xi_0, \varsigma)/d\varsigma|$, where $\partial u/\partial\varsigma$ is infinite. Before this point is reached the ordering assumed for the independent variables, i.e., that $\partial/\partial\varsigma = O(\delta)$, breaks down. Inclusion of the dispersive term prevents the shock from forming. Indeed, Eq. (13) when treated as an initial value problem in ξ is well-posed in an infinite domain in ξ. Although Eq. (6) with the correct boundary conditions is different from Eq. (13) with initial conditions, it is likely that Eq. (6) is also ill-posed if the dispersive term is ignored and if the width of the domain in ξ is large enough.

IV. NUMERICAL RESULTS

We investigate the solution to Eq. (6) by numerically solving Eq. (9) with boundary and initial conditions

$$V(0 < \xi < \xi_1, \tau = 0) = 0, \tag{15a}$$

$$V(\xi = 0, \kappa > 0, \tau > 0) = v_0 \pi\, u(\kappa - \kappa_0)(\kappa - \kappa_0) \exp[-\tfrac{1}{4}(\kappa - \kappa_0)^2], \tag{15b}$$

$$V(\xi = \xi_1, \kappa < 0, \tau > 0) = 0, \tag{15c}$$

where u is the unit step function, v_0 and κ_0 are real constants and $\kappa_0 \geq 0$. The method of solution is given in Appendix A. Without loss of generality, we have taken $\tau_0 = \xi_0 = 0$. In ζ space Eq. (15b) becomes

$$v(\xi = 0)|_{\kappa>0} = v_0[1 + \zeta Z(\zeta)] \exp(i\kappa_0 \zeta)$$

where Z is the plasma dispersion function. With this form of the boundary conditions, we now have three parameters to vary: v_0, κ_0, and $\Delta\xi \equiv \xi_1 - \xi_0 = \xi_1$. The geometry of the waveguide array which might give this input spectrum will be discussed in Sec. V.

We begin by considering the linear non-dispersive limit; i.e., we remove the third and fourth terms in Eq. (6a). Figure 1 shows the solution at various times. Early in the evolution of the waves, only the lowest κ components have propagated throughout the plasma because these have the greatest group velocities. Later on, the other κ components have had time to reach the far end of the system, and the steady state is attained. As $\tau \to \infty$, we have $v = v(\zeta)$. In the original (x, z) coordinate system, this corresponds to the familiar propagation along resonance cones.

In order to further diagnose the results, we identify three sets of waves, the incident waves ($\xi = 0$ and $\kappa > 0$), the reflected waves ($\xi = 0$ and $\kappa < 0$), and the transmitted waves ($\xi = \xi_1$ and $\kappa > 0$). With our choice of boundary conditions the incident waves are constant for $\tau > 0$ and there are no waves incident at the boundary $\xi = \xi_1$. We define reflection and transmission coefficients, R and T, as the ratios of the instantaneous power reflected and the instantaneous power transmitted to the incident power. These powers are defined by integrating $\mathcal{P}$ over the appropriate segment of the boundary. Note that, because energy can be stored in the plasma, we need not have $R + T = 1$, although this is true in a time-averaged sense. Furthermore, it is possible that R or T can momentarily exceed unity. In order to determine where in κ space the power is concentrated, we define $\langle\kappa\rangle$ for each wave component as the ratio of the force to the power for that component. (Since $\mathcal{P} = |V|^2/\kappa$ and $\mathcal{F} = |V|^2$, this ratio has the dimensions of κ.)

For the case shown in Fig. 1, R is obviously zero and the average κ of the reflected waves, $\langle\kappa\rangle_r$, is undefined. Figure 2 shows T and the average κ of the transmitted waves, $\langle\kappa\rangle_t$, for this case. The transmission coefficient T rises in steps as each κ mode reaches the far boundary. [Because of the use of periodic boundary conditions in the numerical solution of Eq. (6), there are only a discrete set of κ modes.] Similarly, $\langle\kappa\rangle_t$ rises with time since modes with higher values of κ take longer to traverse the domain. As $\tau \to \infty$, T approaches unity, signifying total transmission, and $\langle\kappa\rangle_t$ approaches $(\pi/2)^{1/2} \approx 1.25$ which is the same as the average value of κ for the incident waves, $\langle\kappa\rangle_i$.

We now turn to the nonlinear dispersive problem. Because we expect that the effect of the nonlinearity will increase with both v_0 and $\Delta\xi$, we begin with a case where these quantities are chosen small

enough that the nonlinearity only weakly modifies the propagation. Figure 3 shows the solution for such a case with $v_0 = 3$, $\kappa_0 = 0$, and $\Delta\xi = 0.1$. It is found that v attains a steady state by $\tau = 2$ approximately and only this state is shown in Fig. 3. The evolution to this steady state is similar to that for the linear equation. In Fig. 4 are displayed the reflection and transmission coefficients. Note that the reflection coefficient settles down to a small value (somewhat less than 2%).

As the amplitude of the boundary value v_0 is increased, the solution exhibits quite different behavior from the linear solution. In Fig. 5, we have chosen the same parameters as in Fig. 3, except that v_0 has been increased to 4. Now v appears never to reach a steady state, but instead oscillates in some aperiodic fashion. This can be seen in Fig. 6, where R, T, $\langle\kappa\rangle_r$, and $\langle\kappa\rangle_t$ are plotted. From Fig. 5, we can see what is happening during these oscillations. Various κ components in the forward wave nonlinearly interact to produce a reflected wave [Fig. 5(b)]. This interaction causes a severe depletion of the low κ components of the forward wave and transfer of this energy into higher κ components of the forward wave and into the reflected wave [Fig. 5(c)]. After the interaction has nearly gone to completion, the nonlinearly excited components of the field transit out of the system and the fields relax to a state in which there is little variation in $|V|$ with ξ [Fig. 5(d)]. The nonlinear interaction then begins again and the cycle approximately repeats itself [Fig. 5(e)]. In ζ space, this interaction is manifested by a narrowing and peaking of the electric field amplitude v. A typical field pattern is shown in Fig. 5(f).

Returning to Fig. 6, we see that the reflection is appreciable, oscillating around about 20%. Correspondingly, T oscillates around 80%. Because the energy stored in the field comes out in bursts, T is occasionally greater than unity. Finally, we note that $\langle\kappa\rangle_t$ exceeds $\langle\kappa\rangle_i \approx 1.25$ by approximately a factor of 2.

Because the long-time solution of the fields does not reach a steady state, it is useful to describe the solution in terms of its temporal spectrum. To do this, we take a time record of the transmitted and reflected waves for $\tau_a < \tau < \tau_b$. We choose τ_a to be large enough for the transients to have disappeared from the solution and $\tau_b - \tau_a$ to be large enough to include several oscillations of the solution. Effects arising from the finite record length $\tau_b - \tau_a$ are partially eliminated by multiplying by a cosine window $\frac{1}{2}\{1 - \cos[2\pi(\tau - \tau_a)/(\tau_b - \tau_a)]\}$. The resulting function is then transformed in time using a discrete Fourier transform to give the output spectrum $V(\xi', \kappa, \sigma)$ where σ is the slow frequency variable (conjugate with τ), $\xi' = \xi_l$ for $\kappa > 0$ (the transmitted wave), and $\xi' = 0$ for $\kappa < 0$ (the reflected wave). [We assume a space-time dependence of $\exp(i\kappa\zeta - i\sigma\tau)$.]

In Fig. 7, we plot the output spectrum $V(\xi', \kappa, \sigma)$ for the case shown in Figs. 5 and 6. The spectrum is computed between $\tau_a = 1$ and $\tau_b = 5$. The large peaks at $\sigma = 0$ are the steady-state components of the transmitted and reflected waves. The broad spectrum in σ is symptomatic of the aperiodic nature of the waves. There is an interesting correlation in the spectrum: the positive frequency (σ) components of both the transmitted and reflected waves tend to have larger values of $|\kappa|$ than the negative frequency components.

We have seen that the solution becomes more turbulent and that the reflection increases as v_0 is increased. The other parameters that may be varied are $\Delta\xi$ and κ_0. We now investigate the influence of these parameters.

We begin by varying $\Delta\xi$. Figure 8 shows the output spectrum for $v_0 = 4$, $\kappa_0 = 0$ and $\Delta\xi = 0.05$. We see that there is almost no energy in the components of the wave with $\sigma \neq 0$; i.e., the

fields nearly reach a steady state. The reflection coefficient is smaller than in the previous case (where $\Delta\xi = 0.1$) being approximately 4%. Similarly $\langle\kappa\rangle_t$ is only slightly greater than $\langle\kappa\rangle_i$ (1.4 as compared to 1.25). On the other hand, if we increase the value of $\Delta\xi$ to 0.2 (twice its value in Fig. 7), a broad turbulent spectrum is recovered (Fig. 9). Although R and $\langle\kappa\rangle_t$ have approximately the same values as for $\Delta\xi = 0.1$, there is now more energy in the non-steady components of the output spectrum.

Figures 10 and 11 show the effect on the output spectrum of increasing κ_0 (keeping $v_0 = 4$ and $\Delta\xi = 0.1$). In Fig. 10, where $\kappa_0 = 1$, we see that spectrum consists of a few narrow bands indicating that the solution is nearly periodic. Furthermore, the reflected wave consists almost entirely of negative frequency components. The reflection coefficient for this case is about 12%, or half of what it was with $\kappa_0 = 0$. The increase of $\langle\kappa\rangle_t$ over $\langle\kappa\rangle_i$ is moderate (about 3 as compared to 2.42). Increasing κ_0 to 2 (Fig. 11), we see much the same picture except that the frequency of the oscillations is higher. The reflection coefficient of is further reduced to 7% and there is now little difference between $\langle\kappa\rangle_t$ and $\langle\kappa\rangle_i$.

V. THRESHOLD FOR THE NONLINEARITY

In the case shown in Figs. 5–7, the nonlinearity causes three phenomena of importance to lower hybrid heating experiments: (1) the reflection coefficient is appreciable; (2) the solution reaches a turbulent state; (3) the mean wavenumber of the waves transmitted into the plasma is increased. Comparing the results presented here with those of Sec. VIII of Ref. 7 in which the solution of the steady-state problem was attempted, we see that the conditions for the occurrence of these phenomena closely agree with the conditions under which the steady-state problem had no solution and reflection was large.

Before quoting the threshold results from Ref. 7, we use the scaling invariance Eq. (8) to rewrite the boundary condition Eq. (15b) as

$$V(\xi = 0, \kappa > 0, \tau > 0) = v_0 \pi\, u(\kappa - \kappa_0)(\kappa - \kappa_0)\,\Delta\zeta^2 \exp[-\tfrac{1}{4}\Delta\zeta^2(\kappa - \kappa_0)^2].$$

In real space, we have

$$v(\xi = 0)|_{\kappa>0} = v_0[1 + (\zeta/\Delta\zeta)Z(\zeta/\Delta\zeta)]\exp(i\kappa_0\zeta).$$

This roughly corresponds to excitation of lower hybrid waves by a waveguide array of width $\Delta\zeta$. The amplitude of the electric field in the plasma is v_0 and the phasing of the waveguides is such as to give a wavenumber of κ_0. Thus, if the waveguides are phased $0, \pi, 0, \pi, \ldots$, we have $\kappa_0 = \pi M/\Delta\zeta$ where M is the number of waveguides. [The average wavenumber of the spectrum of a single lower hybrid ray is $\langle\kappa\rangle_i$ which, for M large, is approximately $\kappa_0 + 2(2/\pi)^{1/2}/\Delta\zeta$. The first term is attributable to the phasing of the waveguides and the second term arises because of the finite width of the waveguide array.]

For these boundary conditions, the threshold conditions given in Ref. 7 are

$$v_0 \gtrsim 2\kappa_0, \tag{16a}$$

$$\Delta\xi \gtrsim \sqrt{2}v_0^{-3}. \tag{16b}$$

The latter conditions is only correct for M small ($\lesssim 4$). For larger values of M, it should be replaced by

$$\Delta\xi \gtrsim \Delta\zeta\, v_0^{-2}, \tag{16c}$$

which specifies that $\Delta\xi$ should exceed the distance for a shock to form in the dispersionless equation (14). Equation (16) gives the conditions under which the three phenomena described at the beginning of this section occur.

If we now undo the normalizations using Eq. (7), we find that Eq. (16) becomes

$$E_{z0}\,\delta z/T_e \gtrsim 4\sqrt{3}\pi, \tag{17a}$$

$$\Delta x \gtrsim 4\sqrt{6}(T_e/E_{z0})/\beta, \tag{17b}$$

$$\Delta x \gtrsim g\,\Delta z/\beta, \tag{17c}$$

where E_{x0} and E_{z0} are the electric field amplitudes perpendicular and parallel to the magnetic field (so that $E_{z0} = gE_{x0}$), Δz is the width of the waveguide array, $\delta z = \Delta z/M$ is the width of a single waveguide (assuming a $0, \pi, 0, \pi, \ldots$ phasing), Δx is the width of the nonlinear region of the plasma in the x direction, and β is $\frac{1}{4}\epsilon_0 E_{x0}^2/n_0 T_i$, the ratio of the electric field energy to the plasma kinetic energy.

VI. DISCUSSION

We have examined the nonlinear evolution of a lower hybrid wave in two dimensions and time. Under the conditions given in Eq. (17), the nonlinearity can cause appreciable reflection, turbulent variation in the fields, and an increase the wavenumbers of the transmitted waves. In Ref. 7, it was found that these conditions could be satisfied in a small laboratory plasma or near the edge of a tokamak plasma. In such circumstances, the assumption of a steady state and the analyses in Refs. 5-7 based on this assumption are wrong.

The most important application of lower hybrid waves is for heating a tokamak plasma to ignition temperatures. It is therefore important to understand the processes that may modify the lower hybrid waves before they have penetrated to the center of the plasma. Unfortunately, it is not possible to obtain quantitative estimate of these effects with the theory as outlined in the preceding sections. The reason is that, as we have pointed out, the nonlinearity is only important in a tokamak near the edge of the plasma and in that region many other physical processes are likely to be involved. Examples of effects which should probably be included to give a full understanding of lower hybrid wave propagation near the edge are: nonlinear coupling to the second (left-going) ray; electromagnetic effects; density and temperature gradients; saturation of the nonlinearity; ion inertia in the low frequency equations; coupling to low-frequency drift waves.

Although Eq. (6) should be regarded as a very simplified model equation describing the propagation of lower hybrid waves near the edge of a tokamak plasma, some of the phenomena predicted by this equation have been observed in the lower hybrid heating experiment on Alcator–A.[14, 15] The CO_2-laser scattering diagnostic on that experiment indicated a broadening of the frequency spectrum of the waves. This is consistent with the turbulent spectra seen in the solutions of Eq. (6). Furthermore, the spectrum becomes asymmetric as the wave propagates into the plasma, the peak of the spectrum being shifted down from the frequency of the injected waves. This may be a result of the observation in Sec. IV that the components of the transmitted and reflected waves which are down-shifted in frequency have a smaller (in absolute value) wavenumber than those which are up-shifted. If those waves with higher

wavenumbers are preferentially damped as the wave travels into the plasma (e.g., by electron Landau damping), we would expect to see a net downwards shift in the spectrum of waves.

The other somewhat puzzling result of the Alcator-*A* experiment was the apparent independence of the heating results to the phasing of the waveguides. In addition, in order to explain the density dependence of the heating results, it was postulated that the n_z (parallel index of refraction $k_z c/\omega$) spectrum of the waves was shifted to being peaked at around $n_z = 5$ irrespective of the phasing of the waveguides. (This is to be compared with values of n_z predicted on the basis of linear theory of less than 1.5 for the waveguides in phase and of 3 for the waveguides out of phase.) Again, this is qualitatively in agreement with the theoretical results of Sec. IV. There, the average wavenumber of the waves transmitted from the nonlinear region into the center of the plasma was roughly twice that of the wave injected into the nonlinear region when $\kappa_0 = 0$ (corresponding to the wave guides being in phase). As the phase difference between neighboring waveguide becomes finite (i.e., as κ_0 is increased), the amount by which the wavenumber spectrum is shifted is reduced.

It is not clear whether the nonlinear reflection predicted by the theory given in this paper would be observed as an increase in the reflected power measured in the waveguides. It may be that this power is reflected again on the cutoff at $\omega = \omega_{pi}$ very close to the plasma edge. This would convert the power into the other lower hybrid ray.

Thus, it appears that the physics included in Eq. (6) may be responsible for some of the results of the Alcator-*A* experiment. In order to be able to say definitively whether or not the experimental observations are a result of the processes included in Eq. (6), the theory would have to be refined to a point where quantitative comparisons are possible.

We should point out that other theories have been advanced to explain the Alcator-*A* results. In particular, Bonoli and Ott[16] have suggested a linear theory. This is supported by the observed linear dependence between the density fluctuations and the applied power (over a fairly large range) which suggests either that the phenomena are linear or else that the nonlinear processes saturate at a low amplitude.

Another interesting theoretical result, given by Morales,[17] concerns the coupling of rf energy into lower hybrid waves at the plasma edge. A density gradient was included in his model and a temporal evolution was allowed. As in the theory presented here, it was found that a steady state need not be reached; rather, the rf energy entered the plasma in bursts similar to the behavior seen in Fig. 5. However, only a single n_z component was included so that the nonlinear coupling of different n_z components was disallowed.

In summary, we have presented a theory of the nonlinear propagation of lower hybrid waves. At sufficiently large powers, the fields become turbulent and the wavenumber spectrum is shifted upwards. The theory should accurately describe the propagation in small laboratory devices. While we may expect qualitatively similar results near the edge of a tokamak plasma, other physical effects need to be included to obtain an accurate description of the lower hybrid fields in this region.

ACKNOWLEDGMENTS

I wish to thank my collaborators on Ref. 7, F. Y. F. Chu and A. Sen, who encouraged this extension of our earlier work and who helped in its formulation. I would also like to thank N. J. Fisch for extensive discussions and R. H. Berman for his comments on a preliminary version of this paper.

This work was supported by the U.S. Department of Energy under Contract DE–AC02–76–CH03073.

APPENDIX A: NUMERICAL PROCEDURE FOR SOLVING EQ. (6)

The numerical solution of Eq. (6) is carried out in Fourier space so that Eq. (6) becomes Eq. (9). Periodic boundary conditions are used in the ς direction, $v(\xi, \varsigma + L, \tau) = v(\xi, \varsigma, \tau)$; therefore, the Fourier spectrum is discrete the spacing between modes being $\delta\kappa = 2\pi/L$. We use n points to describe v over a single period L. Transformations between the κ and ς spaces are achieved using a discrete Fourier transform. Thus, V is approximated by n Fourier modes. The ξ coordinate is approximated by a grid whose spacing is $\delta\xi$. This equation is solved by splitting each time step $\delta\tau$ into two equal pieces and by approximating Eq. (9a) in the interval $0 \leq \tau < \delta\tau$ by

$$V_\tau = -2 \times \begin{cases} cV_\xi, & \text{for } 0 \leq \tau < \frac{1}{2}\delta\tau, \\ i\Omega V + iN(V), & \text{for } \frac{1}{2}\delta\tau \leq \tau < \delta\tau. \end{cases} \tag{A1}$$

(For simplicity, we describe the solution only for the first time step. The extension beyond this is obvious.)

In each half time step this equation is a partial differential equation in only two independent variables. During the first half time step, κ is merely a parameter and we have a simple linear wave equation to solve. We approximate $V' \equiv V(\tau = \frac{1}{2}\delta\tau)$ as given by Eq. (A1) by shifting $V(\tau = 0)$ over $C = c\delta\tau/\delta\xi$ grid positions. This step is exact if C is an integer. Normally, this is not the case and in that event we interpolate between neighboring grid points. We use linear interpolation on the quantities $|V|^2$ and $|V|^2 \arg V$. This ensures that in this step energy and momentum are conserved. The reason for interpolating in $|V|^2 \arg V$ rather than $\arg V$ is that in the former case the ambiguity of the argument of $V = 0$ is irrelevant. The grid positions within C of the boundary are set to the boundary value.

During the second half time step we have to solve the nonlinear Schroedinger equation at each position ξ. The method is similar to that used in Ref. 7 to solve the steady-state equation (13). The dispersive term is treated exactly and the nonlinear term is treated with a second-order Runge-Kutta scheme. Thus, $V(\tau = \delta\tau)$ is approximated by

$$V'' = BV' + DN(V'),$$
$$V(\delta\tau) = BV' + \tfrac{1}{2}D[N(V'') + N(V')],$$

where $B = \exp(-i\Omega\,\delta\tau)$ and $D = -(1 - B)/\Omega$. The nonlinear term $N(V)$ is calculated by transforming V into v using the discrete Fourier transform, computing $-|v|^2 v$, and transforming back into κ space. In order to avoid problems of aliasing in the computation of $N(V)$, the highest $n/2$ Fourier modes are artificially set to zero.

The accuracy of the numerical integration is checked using the momentum- and energy-conservation laws. Specifically, the time integrals of Eqs. (11) and (12) are numerically computed. These are divided by the total momentum input into the plasma (at $\xi = \xi_0$) and by the total energy injected into the plasma (both at $\xi = \xi_0$, $\kappa > 0$ and at $\xi = \xi_1$, $\kappa < 0$) to provide two measures of the accuracy of the numerical integration, $\Delta\mathcal{M}$ and $\Delta\mathcal{E}$.

The results presented in Sec. IV were (with the exception of Figs. 1 and 2) computed with $n = 2^8$, $L = 20$, and $\delta\xi = 10^{-3}$. The time step was taken to be $\delta\tau = 10^{-3}$ in Figs. 5-7, and 9, $\delta\tau = 2 \times 10^{-3}$ in Figs. 8, 10, and 11, and $\delta\tau = 5 \times 10^{-3}$ in Figs. 3 and 4. The error parameters $\Delta\mathcal{M}$ and $\Delta\mathcal{E}$ were less than about 5×10^{-4} at $\tau = 5$ in all these cases.

The case shown in Figs. 5–7 was also computed with $n = 2^9$, $L = 20$, and $\delta\tau = \delta\xi = 5 \times 10^{-4}$ (i.e., the grid spacing was halved in τ, ζ, and ξ). The solution agreed well with the solution obtained using the coarser grid until about $\tau = 1.5$. Thereafter, the solutions diverged from each other. This is to be expected in a system which exhibits turbulent solutions because the solution is typically very sensitive to the initial conditions. Numerical errors, which have an effect similar to changing the initial conditions slightly, can therefore lead to large changes in the solution. However, although the detailed solution is different after $\tau = 1.5$ in these two cases, the general character of the solution is the same. Thus, the output spectrum for the case with the finer grid spacing shows the same features as the spectrum given in Fig. 7.

References

[1]T. H. Stix, Phys. Rev. Lett. **15**, 878 (1965).

[2]H. H. Kuehl, Phys. Fluids **5**, 1095 (1962).

[3]R. K. Fisher and R. W. Gould, Phys. Rev. Lett. **22**, 1093 (1969) and Phys. Fluids. **14**, 857 (1971).

[4]R. J. Briggs and R. R. Parker, Phys. Rev. Lett. **29**, 852 (1972).

[5]G. J. Morales and Y. C. Lee, Phys. Rev. Lett. **35**, 930 (1975).

[6]H. H. Kuehl, Phys. Lett. **61A**, 235 (1977).

[7]C. F. F. Karney, A. Sen, and F. Y. F. Chu, Phys. Fluids **22**, 940 (1979).

[8]P. M. Bellan and M. Porkolab, Phys. Fluids, **17**, 1592 (1974).

[9]A. I. Akhiezer, I. A. Akhiezer, R. V. Polovin, A. G. Sitenko, and K. N. Stepanov, *Collective Oscillations in a Plasma*, translated by H. S. H. Massey (M.I.T. Press, Cambridge, Mass., 1967).

[10]A. G. Litvak, Izv. VUZ. Radiofizika **9**, 527 (1966) [Soviet Radiophysics **9**, 900 (1966)].

[11]H. C. S. Hsuan, Phys. Rev. **172**, 137 (1968).

[12]V. E. Golant, Zh. Tekh. Fiz. **41**, 2492 (1971) [Sov. Phys. Tech. Phys. **16**, 1980 (1972)].

[13]A. C. Scott, F. Y. F. Chu, and D. W. McLaughlin, Proc. IEEE **61**, 1443 (1973).

[14]J. J. Schuss, S. Fairfax, B. Kusse, R. R. Parker, M. Portolab, D. Gwinn, I. Hutchinson, E. S. Marmar, D. Overskei, D. Pappas, L. S. Scaturro, and S. Wolfe, Phys. Rev. Lett. **43**, 274 (1979).

[15]C. M. Surko, R. E. Slusher, J. J. Schuss, R. R. Parker, I. H. Hutchinson, D. Overskei, and L. S. Scaturro, Phys. Rev. Lett. **43**, 1016 (1979).

[16]P. T. Bonoli and E. Ott (to be published).

[17]G. J. Morales, Phys. Fluids **20**, 1164 (1977).

Tables

TABLE I. Conservation laws for Eq. (6). The form of the conservation laws is $\partial T_j/\partial\tau + \partial X_j/\partial\xi + \partial Z_j/\partial\zeta = 0$. Here q is given by $q_\zeta = v$.

j	T_j	X_j	Z_j
1	iv_ζ	$-v$	$v_{\zeta\zeta} + \lvert v\rvert^2 v$
2	$-iv^* v_\zeta$	$\lvert v\rvert^2$	$3\lvert v_\zeta\rvert^2 - \lvert v^2\rvert_{\zeta\zeta} - \frac{3}{2}\lvert v\rvert^4 + iv v_\tau^*$
3	$iv^* v_\xi$	$\lvert v_\zeta\rvert^2 - \frac{1}{2}\lvert v\rvert^4 - iv^* v_\tau$	$-2\,\mathrm{Re}(v_\xi^* v_\zeta) + \lvert q_\xi\rvert^2$
4	$\lvert v\rvert^2$	$-iq^* v$	$2\,\mathrm{Im}(v^* v_\zeta) + iq^* q_\xi$

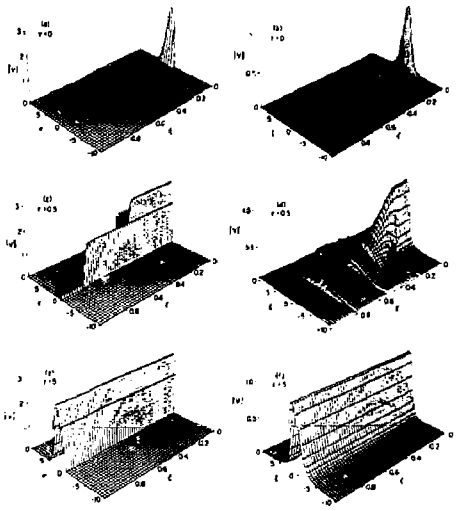

(PPPL-802159)

FIG. 1. The solution to Eq. (6) with the last two terms omitted. Here $v_0 = 1$, $\kappa_0 = 0$, and $\Delta\xi = 1$. The solution is shown in both the κ and ζ spaces for [(a) and (b)] $\tau = 0$, [(c) and (d)] $\tau = 0.5$, and [(e) and (f)] $\tau = 5$.

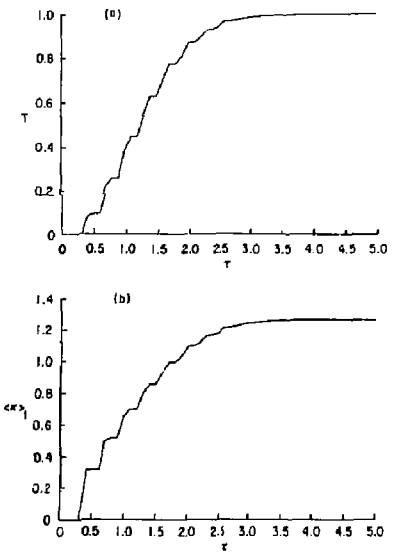

(PPPL-802155)

FIG. 2. The reflection coefficient R (a) and mean value of κ transmitted $\langle\kappa\rangle_t$ (b) as functions of time for the case shown in Fig. 1.

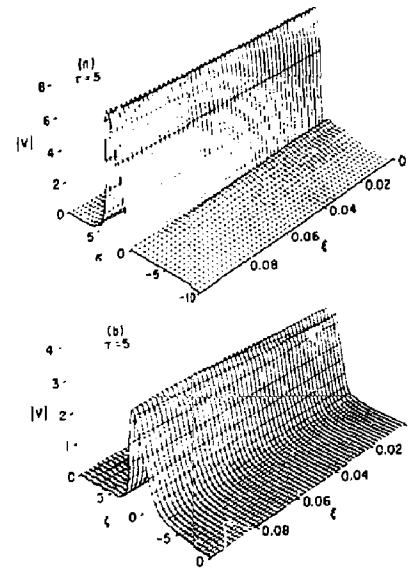

(PPPL-802156)

FIG. 3. The solution to Eq. (6) for $v_0 = 3$, $\kappa_0 = 0$, and $\Delta\xi = 0.1$. The solution is shown for $\tau = 5$ in (a) κ space and (b) ζ space.

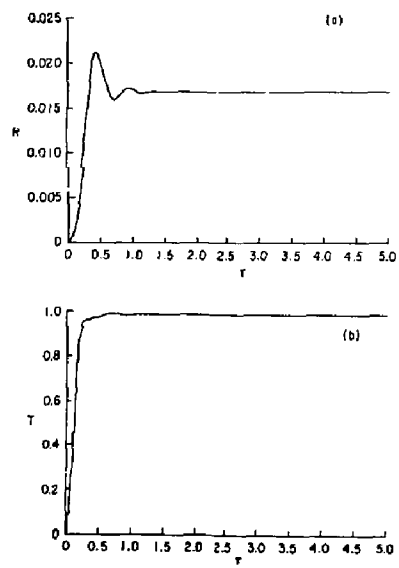

(PPPL-802158)

FIG. The reflection (a) and transmission (b) coefficients, R and T, as functions of time for the case shown in Fig. 3.

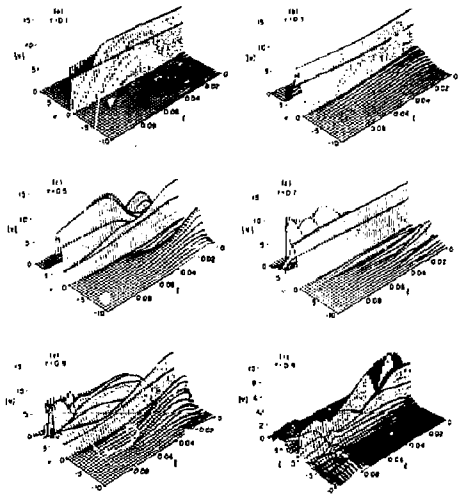

(PPPL-802160)

FIG. 5. The solution to Eq. (6) for $\kappa_0 = 4$, $\kappa_0 = 0$, and $\Delta\xi = 0.1$. The solution is shown in κ space for (a) $\tau = 0.1$, (b) $\tau = 0.3$, (c) $\tau = 0.5$, (d) $\tau = 0.7$, (e) $\tau = 0.9$, and in ζ space for (f) $\tau = 0.9$.

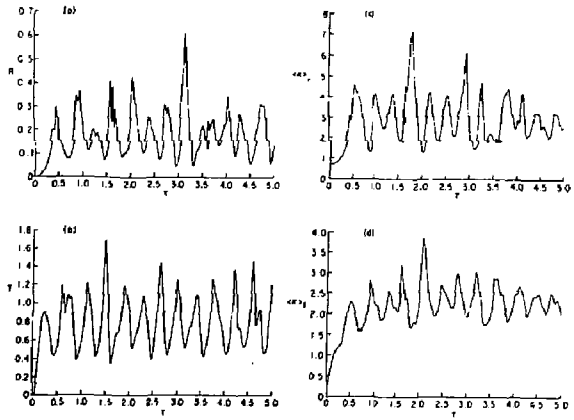

(PPPL-802157)

FIG. 6. The output waves as functions of time as described by (a) R, (b) T, (c) $\langle\kappa\rangle_\tau$, and (d) $\langle\kappa\rangle_t$.

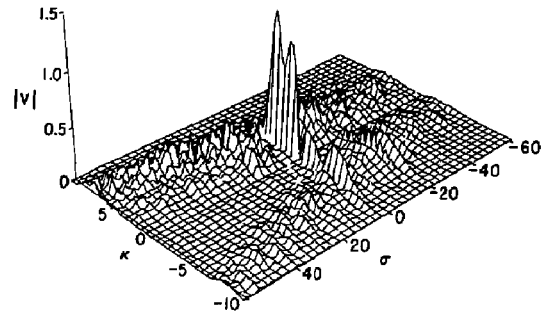

(PPPL-802164)

FIG. 7. The output spectrum for the case shown in Figs. 5 and 6. Here and in the remaining figures the spectrum is computed with $\tau_a = 1$ and $\tau_b = 5$.

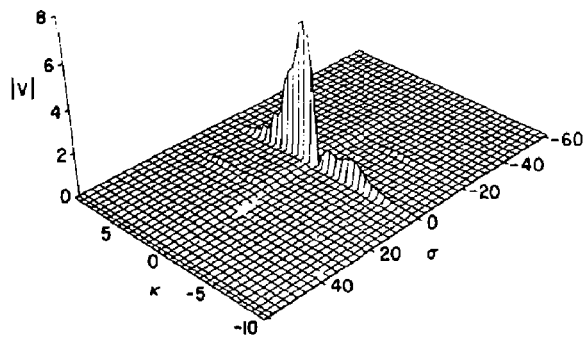

(PPPL-802154)

FIG. 8. The output spectrum for $\nu_0 = 4$, $\kappa_0 = 0$, and $\Delta\xi = 0.05$.

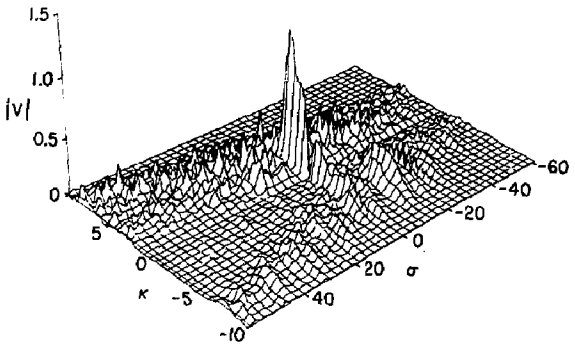

(PPPL-802151)

FIG. 9. The output spectrum for $v_0 = 4, \kappa_0 = 0$, and $\Delta\xi = 0.2$.

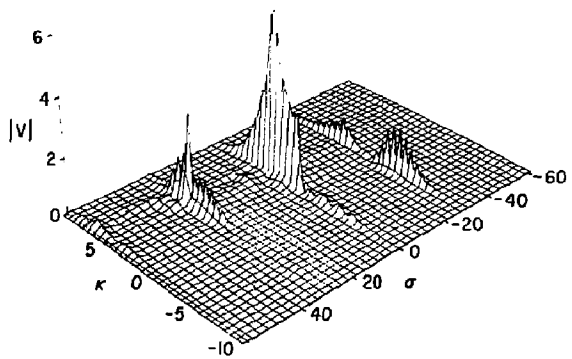

(PPPL-802152)

FIG. 10. The output spectrum for $v_0 = 4, \kappa_0 = 1$, and $\Delta\xi = 0.1$.

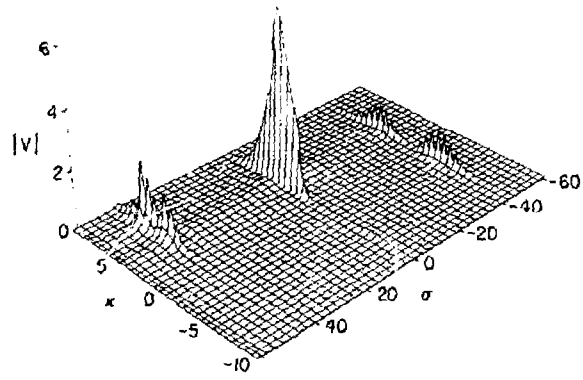

(PPPL-802153)

FIG. 11. The output spectrum for $v_0 = 4$, $\kappa_0 = 2$, and $\Delta\xi = 0.1$.